# Ionization of a hydrogenic ion by electron and positron impact in the presence of a laser field

A. Chattopadhyay and C. Sinha
*Department of Theoretical Physics, Indian Association for the Cultivation of Science, Jadavpur, Kolkata 700032, India*
(Received 6 June 2005; published 11 November 2005)

The modification due to an external linearly polarized monochromatic laser field in the dynamics of the ionization process of a hydrogenic ion by electron and positron impact is studied theoretically for coplanar geometry. Significant changes are noted both in the shape and magnitude of the triple-differential cross sections (TDCS) by the application of the laser field. The net effect of the laser field is to suppress the field-free (FF) cross sections in the zeroth-order approximation of the ejected electron wave function, while in the first order the cross sections are found to be enhanced or suppressed depending on the kinematics of the process. The TDCS is found to be quite sensitive with respect to the initial phase as well as the frequency of the laser field. For positron impact, the effect of the laser field on the dynamics of the electron capture to continuum (ECC) phenomena is also studied. No significant change is noted in the qualitative behavior of the FF ECC peak with the application of the laser field.

DOI: 10.1103/PhysRevA.72.053406 PACS number(s): 34.80.Qb

## I. INTRODUCTION

Laser-assisted ionization of positive ions by charged particles, (e.g., electron, positron, etc.) plays a very prominent role in many practical fields, such as in the plasma confinement in fusion plasma, laser heating of plasma, high-power gas lasers, etc. In particular, such collision cross sections are highly needed in the study of laser-produced plasma. In view of the recent availability of increasingly more powerful and tunable lasers, both laser-induced and laser-assisted collision phenomena are nowadays being observed in laboratories [1–9]. Until now, these measurements have been limited to neutral targets only, probably because of some technological difficulties associated with the ionic targets. Specifically, the first kinemetically complete experiment due to Höhr *et al.* [10] for the laser assisted single ionization $(e,2e)$ process of He atom has been reported very recently. This measurement indicates a bright future for such a laser-assisted ionization process and inspires the theoreticians along this line, since for them it is much easier to study the fully (triple) differential cross sections rather than the total cross sections, as the latter involve a number of integration steps over the fully differential ones. Further, the fully differential cross sections provide the most detailed information of an ionization process since the characteristic structures of that particular process are smoothed out by the aforesaid integration steps to evaluate the double, single differential, and total ionization cross sections. A number of theoretical calculations [11–19] exist in the literature for the laser-assisted $(e,2e)$ process of H and He atoms, prior to the experiment of Höhr *et al.* [10]. However for the ionic target, even for the simplest $He^+$, no laser-assisted $(e,2e)$ experiment is yet available in the literature. The absence of any experimental data adds further importance to the theoretical study of such a process. Further, due to the laser modification of the ionization cross sections, it might be possible to control the ionization process by a suitable choice of laser parameters as well as the projectile energy, i.e., to enhance or suppress the ionization cross sections as per the requirement in a particular physical process. Since the laser field can act as a reservoir of energy and its polarization vector introduces a new axis of symmetry, the laser-assisted ionization cross sections could differ strongly in shape and magnitude from the field free (FF) cross sections as predicted in the recent measurement [10], as well as in several theoretical studies on this topic [11–19].

The present study addresses the problem of ionization of a ground-state hydrogenic ion $(He^+)$ by electron $(e)$/positron $(e^+)$ impact in the presence of a monochromatic linearly polarized homogeneous laser field. To our knowledge, this work is the first attempt for the laser-assisted ionization process of an ionic target. The calculation is performed in the framework of Coulomb–Born approximation, where the final state involves correlated Coulomb continuum and satisfies the exact asymptotic three-body boundary conditions [20]. In this work, we have studied the modifications of the angular and energy distributions [triple-differential cross section (TDCS)] of the ejected electron in coplanar geometry due to the external laser field.

In the present prescription, the projectile–screened-ion interaction is considered to be the perturbation responsible for the collision, while the role of the external laser field is to modify the projectile electron state as well as the initial bound and continuum states of the target ion. Thus, for a laser-assisted ionization process, the phenomena which have to be considered are the dressing of the initial and final target states as well as the interaction of the charged continuum particles with each other and the laser field.

The wave function of the projectile electron or positron in the combined effect of the long-range Coulomb interaction of the screened target ion and the laser field is assumed in the present model to be of Coulomb–Volkov (CV) type proposed by Jain and Tzoar [21] and later used by several workers [11–13,17,18,22]. Although the approximate CV solution presents the advantage of containing the field in all orders (inherent in the plane-wave Volkov solution [23]), it completely decouples the projectile-laser and projectile–screened ion interaction [14,15]. The laser-ion interaction (i.e., target dressing) is considered to first order only, although the

 

present method can be extended to take account of the higher-order Stark effect as well.

In case of electron impact, the electron exchange effect between the incident and the ejected electrons is neglected in the present work. However, the neglect of exchange could probably be justified by the following fact [22,24]. If the identical particles (here electrons) respond in a different manner to an external driving field (as considered in the present model), the particles, to some extent, become distinguishable.

## II. THEORY

The reaction studied is

$$e^{\mp}(E_i,\vec{k}_i)+A^{(Z-1)+}(1s)\pm\gamma(\omega,\vec{\varepsilon}_0)\rightarrow e^{\mp}(E_1,\vec{k}_1)+e^{-}(E_2,\vec{k}_2)+A^{(Z-2)+} \quad (1)$$

where $E_i$, $E_1$, $E_2$, and $\vec{k}_i$, $\vec{k}_1$, $\vec{k}_2$ are the energy and the momentum of the incoming, scattered charged particles $e^-$ or $e^+$ and ejected electron respectively. $Z$ is the charge of the target ion and $\gamma(\omega,\vec{\varepsilon}_0)$ stands for the laser photon with frequency $\omega$ and field strength $\varepsilon_0$.

The prior form of the $T$-matrix element for the laser-assisted ionization process of a hydrogenic ion is given by

$$T_{if}=-i\int_{-\infty}^{\infty}dt\langle\Psi_f^-|V_i|\psi_i\rangle, \quad (2)$$

where $V_i$ is the perturbation potential in the initial channel. $\Psi_f^-$ in Eq. (2) is an exact solution of the three-body problem satisfying the incoming wave boundary condition, while $\psi_i$ represents the asymptotic initial channel wave function. Only the collision dynamics is treated quantum mechanically whereas the laser field is assumed to be treated classically and is chosen to be single mode, linearly polarized, and spatially homogeneous electric field represented by $\vec{\varepsilon}(t)=\vec{\varepsilon}_0\sin(\omega t+\delta)$. The corresponding vector potential in the Coulomb gauge is $\vec{A}(t)=\vec{A}_0\sin(\omega t+\delta)$, with $\vec{A}_0=c\vec{\varepsilon}_0/\omega$ and $\delta$ is the initial phase of the laser field. For details of the theory, the interested reader is referred back to our earlier paper [22]. The atomic unit (a.u.) system is followed throughout the work.

The initial channel perturbation $V_i$ [in Eq. (2)] which is the part of the total interaction ($V_{\text{int}}$) not diagonalized in the initial state is given by

$$V_i=\mp\frac{1}{r_1}\pm\frac{1}{r_{12}}, \quad (3)$$

where the upper sign always refers to the ($e^-$) impact while the lower sign stands for positron ($e^+$) impact.

It is evident from Eq. (3) that the perturbation $V_i$ vanishes asymptotically (for $r_1\rightarrow\infty$ and $r_2$ finite).

The energy conservation relation for such a laser-assisted ionization process (for transfer of $l$ photons) is given by

$$E=\frac{1}{2}k_i^2+l\omega-\in_i=\frac{1}{2}k_1^2+\frac{1}{2}k_2^2,\quad l=0,\pm1,\pm2,\ldots \quad (4)$$

A major difficulty in the theoretical investigation of such a laser-assisted ionization process is to construct the wave function of the ejected electron in the combined field of the residual target nucleus ($He^{2+}$) and the laser field. The laser-dressed continuum wave function for the ejected electron (with momentum $\vec{k}_2$) $\Phi_{k_2}^d(\vec{r}_2,t)$ in the present work is chosen to be (first proposed by Joachain *et al.* [14,15]),

$$\Phi_{k_2}^d(\vec{r}_2,t)=\exp(-iE_{k_2}t)\exp(-i\vec{a}\cdot\vec{r}_2)\exp[i\vec{k}_2\cdot\vec{\alpha}_0\sin(\omega t+\delta)]\times\left[\psi_{c,k_2}^{(-)}(\vec{r}_2)+\frac{i}{2}\sum_n\left[\frac{\exp[i(\omega t+\delta)]}{E_n-E_{k_2}+\omega}-\frac{\exp[-i(\omega t+\delta)]}{E_n-E_{k_2}-\omega}\right]M_{nk_2}\psi_n(\vec{r}_2)+i\vec{k}_2\cdot\vec{\alpha}_0\sin(\omega t+\delta)\psi_{c,k_2}^{(-)}(\vec{r}_2)\right], \quad (5)$$

where $\psi_{c,k_2}^{(-)}(\vec{r}_2)=(2\pi)^{-3/2}C_2\exp(i\vec{k}_2\cdot\vec{r}_2)\,{}_1F_1(-i\alpha_2,1,-i(k_2r_1+\vec{k}_2\cdot\vec{r}_1))$; $\alpha_2=Z/k_2$; $E_{k_2}$ being the energy of the ejected electron and the Coulomb normalization constant $C_j=\exp(\pi\alpha_j/2)\Gamma(1+i\alpha_j)$, $M_{n,k_2}=\langle\psi_n|\vec{\varepsilon}_0\cdot\vec{r}_2|\psi_{c,k_2}^{(-)}\rangle$, and $\vec{\alpha}_0=\pm\vec{\varepsilon}_0/\omega^2$. The main difficulty lying with the evaluation of Eq. (5) is to perform the infinite summation running over the whole atomic spectrum. To circumvent this difficulty, some sophisticated techniques were adopted for laser-assisted inelastic collisions with neutral targets e.g., Coulomb Green's function [14–16,25,26] for proper evaluation of the infinite summation or a fully nonperturbative Floquet technique [27–29], while, the use of closure approximation [30–32] was questioned by Martin *et al.* [15], particularly for the case of continuum states. However, for the ionic target, even the FF ionization problem is quite difficult to solve rigorously because of the presence of the long-range Coulomb interaction between the projectile and the target. As such, as a first attempt, we resort to closure approximation [30–32] for the evaluation of the infinite summation occurring in Eq. (5), the average excitation energy, $\bar{E}_n$ being chosen to be the ionization energy of target $He^+$ (2 a.u.). As for some justification of the use of closure approximation, it may be pointed out that for $E_n\gg E_{k_2}\pm\omega$ (as happens to be the case in the present work), the contribution of the term containing the infinite summation is negligible as compared to the other two terms in Eq. (5). Further, we have also tested the sensitivity of our calculation by varying the average excitation energy ($\bar{E}_n$) around its expected value (2 a.u.). The results are found to be quite insensitive with respect to the choice of $\bar{E}_n$ which also extends support to the reliability of the present calculation.

It may be noted that the first term of Eq. (5), i.e., the zeroth-order result is reduced to the CV solution. Hereafter, this term will be called as LM0, while the full dressing term for the ejected electron [in Eq. (5)] will be referred to as LM1.

The final state wave function $\Psi_f^-$ in Eq. (2) satisfying the exact asymptotic three-body incoming wave boundary condition for the ionization process is approximated as

$$\Psi_f^- = \Phi_{k_2}^d(\vec{r}_2,t) \times \chi_{k_1}(\vec{r}_1,t) C_{121} F_1(-i\alpha_{12},1,-i(k_{12}r_{12}+\vec{k}_{12}\cdot\vec{k}_{12})), \tag{6}$$

$$\vec{k}_{12} = \frac{1}{2}(\vec{k}_1 - \vec{k}_2), \quad \text{and } \vec{r}_{12} = \vec{r}_1 - \vec{r}_2, \quad \alpha_{12} = \mp \frac{1}{2|\vec{k}_{12}|},$$

where $\chi_{k_1}(\vec{r}_1,t)$ denotes the CV solution for the scattered $e$ or $e^+$ in the final state and is given by

$$\chi_{k_1}(\vec{r}_1,t) = (2\pi)^{-3/2} \exp[i(\vec{k}_1\cdot\vec{r}_1 + \vec{k}_1\cdot\vec{\alpha}_0 \sin(\omega t+\delta) - E_{k_1}t)] \times C_{11} F_1[-i\alpha_1,1,-i(k_1 r_1 + \vec{k}_1\cdot\vec{r}_1)] \quad \text{with } \alpha_1 = \pm \frac{Z}{|\vec{k}_1|}. \tag{7}$$

By virtue of the generating function [22,33], as well as the addition theorem of the Bessel functions [33], the $t$ (time) integration in Eq. (2) is performed analytically to obtain finally (after simplification)

$$T_{if} = -i \sum_l \delta(E_1 + E_2 - E_i - l\omega) J_l(\beta) I, \tag{8}$$

where $\beta = A(\cos\delta + \sin\delta)$; $A = [\vec{k}_i - (\vec{k}_1 + \vec{k}_2)]\cdot\vec{\alpha}_0$ and $I$ stands for the space integral part of the transition matrix element $T_{if}$.

The expression for the TDCS for the process (1) accompanied by the transfer of "$l$" photons is given by

$$\frac{d^3\sigma_{\text{ion}}}{d\Omega_1 d\Omega_2 dE_2} = \frac{k_1 k_2}{k_i} |T_{if}^l|^2. \tag{9}$$

## III. RESULTS AND DISCUSSIONS

We have computed the TDCS for the ionization of a helium ion ($He^+$) from its ground state by electron ($e$) or positron ($e^+$) impact in presence of a monochromatic, linearly polarized laser field at intermediate and high incident energies (e.g., $E_i$=200 eV and 500 eV) in coplanar geometry. Both the asymmetric (unequal energy sharing between the ejected electron and the scattered $e$ or $e^+$) and symmetric geometries (equal energy sharing) are studied. The laser field is chosen to be parallel to the incident momentum direction. The present study concerns the zero-photon transfer ($l$=0), as well as the single-photon absorption or emission ($l=\pm1$) processes. It may be mentioned that, for the present laser parameters, the absorption and emission cross sections are found to be almost identical and as such only the absorption cross sections are presented.

Figures 1–4 demonstrate the angular distributions of the ejected electron (TDCS) for the aforesaid process for asymmetric geometry at incident electron or positron energies 200 eV and 500 eV with a laser frequency of 1.17 eV (in the soft photon limit) and a field strength of $5\times10^9$ V/m (tunable Ti: Sapphire laser, near-infrared region) for zero-photon ($l$=0, Figs. 1 and 2) and single-photon ($l$=1, Figs. 3 and 4) transfer cases.

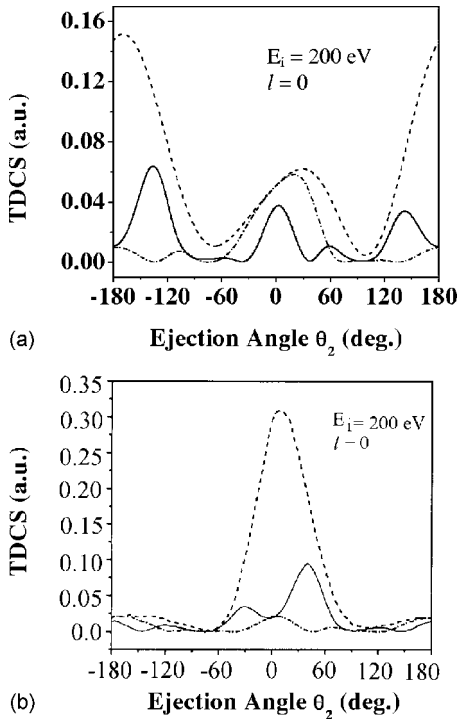


FIG. 1. The TDCS (a.u.) as a function of the ejected electron angle $\theta_2$ for the ionization of $He^+$ ion from the ground state by electron (a)/positron (b) impact in the presence of a laser field. The incident projectile energy is $E_{k_i}$=200 eV. The ejected electron energy is $E_{k_2}$=5 eV and the scattering angle $\theta_1$=3°. Laser parameters used: $\varepsilon_0 = 5\times10^9$ V/m and $\omega$=1.17 eV (Ti: Sapphire laser). The number of photon absorbed is taken to be zero, i.e., $l$=0. Solid curve: Considering full dressing of the ejected electron (LM1), Dash-dot curve: Considering the zeroth-order approximation for the ejected electron (LM0), Dashed curve: The FF TDCS for the ejected electron.

### A. $l$=0 case

As may be noted from Fig. 1(a), the strong recoil peak noted in the FF case at intermediate incident energy (e.g., $E_i$=200 eV) for electron impact ionization of the positive ion $He^+$ [34–36] is strongly suppressed by the application of the laser field, though still maintaining the FF qualitative feature, e.g., the ratio binary peak intensity/recoil peak intensity ($b/r$) is less than one. This behavior (i.e., the intense recoil peak even larger than the binary one) is a peculiarity for an ionic target at lower incident energies and could be attributed [34–36] to the strong elastic scattering of the electron from the nucleus, since the recoil peak is mainly governed by the electron-nucleus interaction. As is revealed from Fig. 1(a), the suppression of the FF binary peak for the $l$=0 case [Fig. 1(a)] is much less as compared to the recoil one, both for the zeroth-order dressing (LM0, dash-dot curve) and the first-order dressing (LM1, solid curve) of the ejected electron, although in the former case (LM0), the reduction is much higher than in the latter.

The TDCS for $e^+$ impact on the other hand, in Fig. 1(b) exhibits the reverse behavior, since for $e^+$ impact at lower incident energy, the FF TDCS is mainly governed by binary collision (i.e., almost recoilless) [34–36], the modification

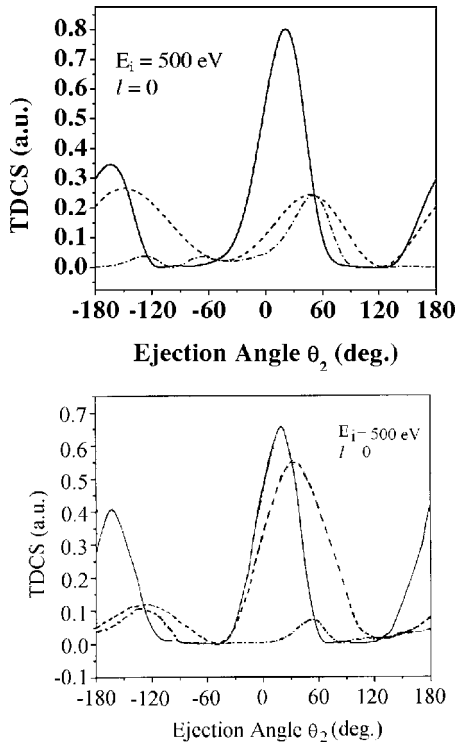


FIG. 2. Same as Fig. 1 but for $E_{k_i}$=500 eV.

(reduction) due to laser field is much more significant for the binary peak as compared to the recoil one.

Figures 2 demonstrates the similar TDCS (as in Figs. 1) for $e$ [Fig. 2(a)] and $e^+$ [Fig. 2(b)] impact but at higher incident energy 500 eV. As may be noted from these figures,

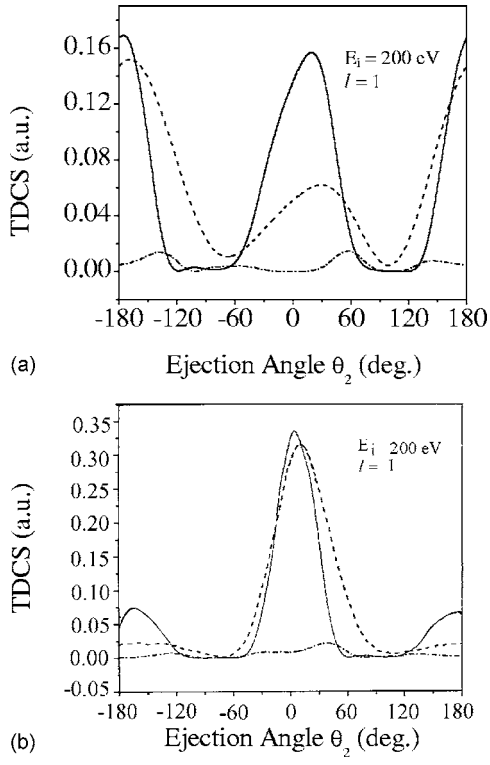


FIG. 3. Same as Fig. 1, except for $l=\pm 1$.

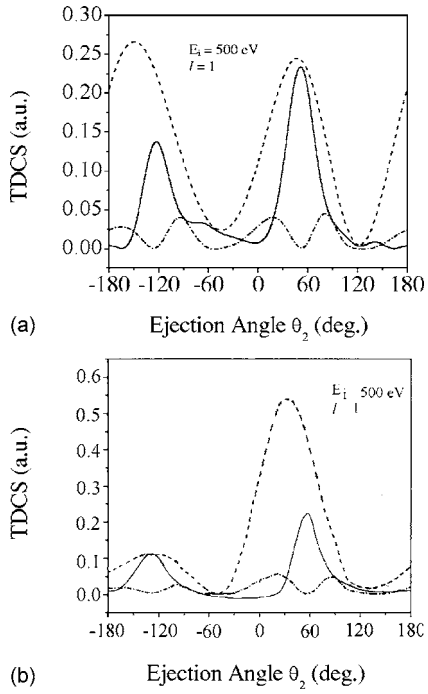


FIG. 4. Same as Fig. 2, except for $l=\pm 1$.

with increasing incident energy, the FF recoil peak becomes more and more prominent for $e^+$ impact [as compared to lower incident energy in Fig. 1(b)], while for $e$ impact, the converse is true, i.e., with increasing incident energy, the magnitude of the recoil peak decreases and the binary peak intensity finally takes over (e.g., for $E_i$=1000 eV not shown in the figure).

On the other hand, for the laser-assisted zero-photon transfer ($l$=0) cases, and for $e$ impact, the LM0 result (dash-dot curve) almost follows the behavior of the FF results in the binary region, while the recoil peak is always [Fig. 2(a)] strongly suppressed, although the suppression becomes lower with increasing incident energy. In contrast, for $e^+$ impact, the converse is true, i.e., the recoil peak is very close to the FF one, while the binary peak is strongly suppressed with respect to the FF one [vide Fig. 2(b)]. Further, some additional structures also appear in the binary region for $e^+$ impact.

Regarding the LM1 results, the electron (position) impact TDCS exhibits somewhat different behavior at lower incident energy (e.g., $E_i$=200 eV in Fig. 1]. For instance, in this case (in contrast to the LM0 results), both the binary and the recoil peaks are suppressed with respect to the FF ones, although the suppression being much more for the recoil (binary) peak. With increasing incident energies ($E_i$=500 eV), on the other hand, the binary and recoil peak intensities are enhanced as compared to the lower-energy case (Fig. 1) for both $e$ and $e^+$ impact (Fig. 2). Further Fig. 2(a) [Fig. 2(b)] also reveals that the electron (positron) TDCS recoil (binary) peak intensity becomes almost comparable, while the binary (recoil) peak intensity gets significantly enhanced as compared to the corresponding FF ones.

Thus, finally, from Figs. 1 and 2, it may be inferred that for $l$=0, due to laser modification, the qualitative behavior of

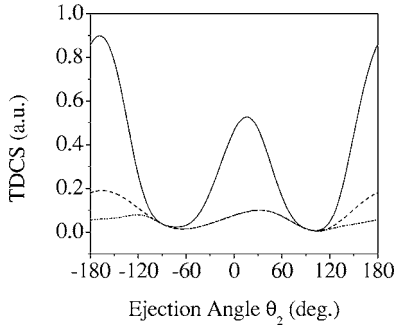


FIG. 5. The TDCS (a.u.) as a function of the ejected electron angle $\theta_2$ for the process (1) with $\varepsilon_0=5\times10^9$ V/m and $\omega=1.17$ eV at $E_i=250$ eV. Dash-dot-dot curve denotes the summed TDCS over $l$ up to $l=\pm3$ for LM0 case. Solid curve denotes the same TDCS for LM1 case. Dashed curve represents the FF results.

the binary and recoil peaks of the $e$ TDCS is just the reverse of the corresponding $e^+$ TDCS (for both LM0 and LM1), as is expected physically.

### B. $l=1$ case

In the case of single-photon transfer ($l=1$), the LM0 TDCS results for both $e$ and $e^+$ impact (Figs. 3 and 4) are strongly suppressed as compared to the corresponding FF results at all the incident energies presented in Figs. 3 and 4. Further, these results exhibit some additional lobes both in the binary and recoil regions as compared to the FF TDCS, the latter possessing only two distinct lobes (binary and recoil). Another distinctive feature noted for LM0 case is that the FF recoil dominance ($b/r<1$) for $e$ impact ionization of $He^+$ ion [34–36] is destroyed by the laser field for single-photon transfer case ($l=\pm1$) at all incident energies. However for $e^+$ impact (unlike $e$ impact) the FF binary dominance is maintained in the LM0 case.

For the LM1 case, on the other hand, the modification due to laser field at $E_i=200$ eV for $e$ impact is in the reverse direction as noted in the $l=0$ case, e.g., both the binary and recoil peaks are enhanced with respect to the corresponding FF case. Further, in this case [Fig. 3(a)], the peak intensity of the recoil peak is very close to that of the binary one (ratio $b/r\approx0.92$) in contrast to the FF ratio $b/r\approx0.41$. With increasing incident energy, the laser modification (LM1) on the binary peak intensity decreases and the ratio $b/r$ changes from $<1$ [at 200 eV in Fig. 3(a)] to $>1$ at $E_i=500$ eV in Fig. 4(a). On the contrary, for $e^+$ impact, $l=1$ TDCS (for LM1) the ratio $b/r$ is $>1$ at all incident energies as in the FF case. The laser field in this case (LM1) enhances all the binary and recoil peak intensities to a small extent at lower incident energy $E_i=200$ eV [Fig. 3(b)]. However, with increasing $E_i$, the FF binary peak is considerably reduced by the laser field. On the other hand, the enhancement of the recoil peak (as noted for $E_i=200$ eV) decreases slowly with increasing $E_i$, so that finally at $E_i=1000$ eV, the laser modified recoil peak intensity becomes lower than the FF one (not shown in the figure).

As in the case of excitation process (e.g., our earlier work [22]), the laser-assisted TDCS can also be related to the FF

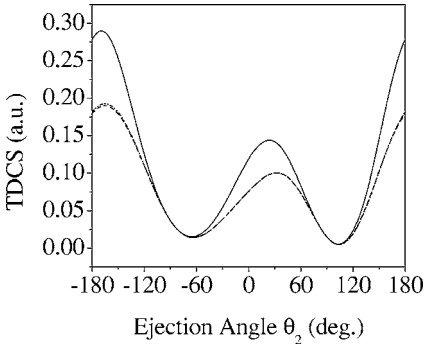


FIG. 6. Same TDCS as in Fig. 5, except with $\omega=2$ eV.

TDCS in the weak-field limit (neglecting target dressings) and in the high-energy Coulomb–Born approximation (i.e., corresponding to on shell matrix element)

$$\sum_{l=-\infty}^{\infty}\left(\frac{d\sigma^l(k_i,k_1(l),k_2(l))}{d\Omega_1 d\Omega_2 dE_2}\right)_{\text{no dressing}} \approx \frac{k_1(l)k_2(l)}{k_i}J_l^2(\vec{q}\cdot\vec{\alpha}_0) \times\left(\frac{d\sigma}{d\Omega_1 d\Omega_2 dE_2}\right)_{CB}. \tag{10}$$

The validity of this sum rule is quite apparent in Figs. 5 and 6, where the number of photon exchange is considered up to $l=\pm3$. Further, with increasing laser frequency $\omega$, the sum rule is attained with smaller number of photon exchange ($l$) than in the case of lower frequency. It may be pointed out here that in both cases (FF and laser-assisted cases), the projectile-electron correlation effect has been taken into account properly (unlike other theoretical laser-assisted $(e,2e)$ processes [11–17]), which is essential for a reliable estimate of the ionization cross sections. Incorporation of target dressing (both in the initial and final channels) shows a significant deviation from the sum rule (10) as may be noted from Figs. 5 and 6.

Figures 7 and 8 illustrate similar TDCS as in Figs. 2 and 4 at $E_i=500$ eV, but for a higher ejection energy, e.g., $E_2=20$ eV for $e$ (Fig. 7) and $e^+$ (Fig. 8) impact. As is evident from the figures, with increasing ejection energy, both the FF binary and recoil peak (particularly the latter one) intensities decrease for both $e$ and $e^+$ impact, although the peak posi-

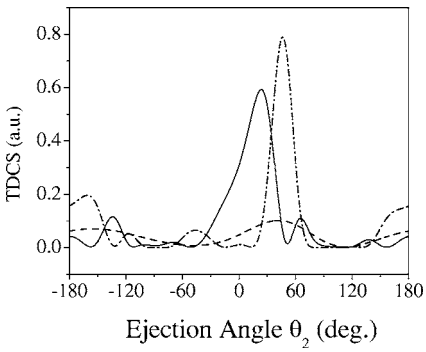


FIG. 7. Same as Figs. 2(a) and 4(a), except for $E_2=20$ eV. Solid curve: LM1 results for $l=1$, dash-dot curve: LM1 results for $l=0$, and dashed curve: FF results.

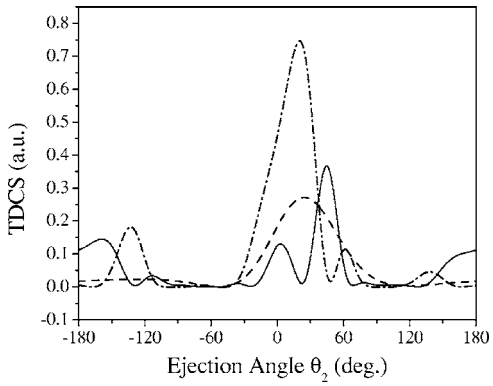


FIG. 8. Same as Fig. 7 except for $e^+$ impact.

tions remain almost the same for lower and higher $E_2$. For higher $E_2$, the behavior of the FF binary and recoil peaks for $e$ impact are reverse as compared to the lower $E_2$ case [Figs. 2(a) and 4(a)], e.g., the ratio $b/r$ is $<1$ for lower $E_2$; while it is $>1$ for higher $E_2$. With the application of the laser field, on the other hand, for $l=0$ case, the ratio $b/r$ is $>1$ for both higher and lower $E_2$ (for the LM1 case). In fact, as noted from Fig. 7, the binary peak intensity is more or less comparable in the two cases (higher and lower $E_2$), while the recoil peak intensity is suppressed for higher $E_2$ as compared to the lower one.

For $l=1$, on the other hand, the binary peak intensity enhances with increasing ejection energy $E_2$. For higher $E_2$, the laser-assisted (LM1) binary peak intensity is even greater than that of the FF one, while for lower $E_2$, the FF and LM1 binary peaks are comparable in magnitude [vide Fig. 4(a)]. As for the recoil peak, the LM1 peak is highly suppressed by the laser field for lower $E_2$, while for higher $E_2$, it is slightly enhanced by the laser field.

Figure 8 demonstrates the corresponding $e^+$ impact TDCS at higher $E_2$ for both zero- and single-photon transfers ($l=0,\pm1$) along with the FF results. As may be indicated from Fig. 8, the laser field (for both $l=0$ and $\pm1$) modifies (enhances) remarkably the binary dominant (recoil less) FF TDCS for higher $E_2$ such that the laser-assisted ionization is now no more recoil less; instead, a significant recoil peak starts showing up when compared with the corresponding FF results. However, the ratio $b/r$ in this case (for $e^+$ impact) is always $>1$ irrespective of the application of the field.

Figure 8 also indicates that for $l=1$, both peak intensities (binary and recoil) get enhanced with respect to the corresponding FF cases for higher ejection energy ($E_2$), while for lower $E_2$ [Fig. 4(b)] the situation is just the reverse. This feature (for $l=1$) may be contrasted with that for $l=0$, where the behavior for higher $E_2$ (Fig. 8) and lower $E_2$ [Fig. 2(b)] is similar in the sense that both are enhanced with respect to the FF case. Further, comparison between Figs. 2(b), 4(b), and 8 reveals that for lower $E_2$, the laser modification is much more for the binary peak than for the recoil one, while it is reverse for higher $E_2$, e.g., the recoil peak is much more affected as compared to the binary one by the external laser field. This behavior holds for both $l=0$ and $\pm1$.

It is also noted from Figs. 7 and 8 that for higher ejection energy ($E_2$), additional structures appear in the binary region

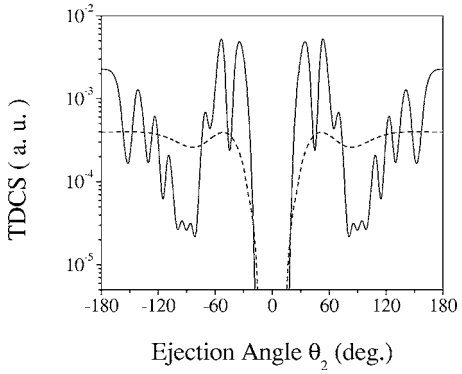


FIG. 9. The TDCS (a.u.) versus $\theta_2$ results for laser assisted (LM1) $e$ impact ionization for symmetric energy sharing. $E_i=254.4$ eV, $E_2=100$ eV, and $\theta_1=0°$. The number of photon transferred is one ($l=\pm1$). Laser parameters are same as in Figs. 1–4. Solid curve: LM1 results, Dashed curve: FF results.

in presence of the laser field, the effect being more prominent for $e^+$ impact single-photon transfer case ($l=\pm1$).

Figures 9 and 10 display the TDCSs for the symmetric geometry when the scattered positron or electron and the ejected electron share identical energy in the final channel (e.g., $E_i=254.4$ eV, $\theta_1=0°$, and $E_1=E_2=100$ eV), the laser parameters are same as in Figs. 1–4. The qualitative behavior corresponding to the zero-photon transfer case ($l=0$) is more or less similar to the $l=1$ case (except for some additional oscillations in the $l=1$ curves) and as such we have omitted the $1=0$ results. As is apparent from the figures, the laser field (LM1) enhances the average binary peak as well as the recoil peak intensities to a considerable extent, for both $e$ and $e^+$ impact. Further, the laser-assisted (LM1) TDCS exhibit some additional structures in the binary and recoil regions particularly at larger ejection angles, for both electron and positron impact.

Another important feature to be mentioned for the symmetric geometry (equal energy sharing) is that for $e^+$ impact, the differential cross section shows (vide Fig. 10) a cusplike (singular) structure when the scattered positron and the ionized electron emerge in the same direction. This behavior may be physically explained as arising due to the process of electron capture to continuum (ECC), where the electron is dragged or captured by the projectile ($e^+$) to its low continuum. The Coulomb density of states factor [vide Eqs. (6)]

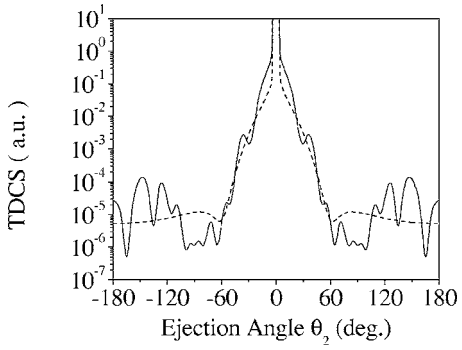


FIG. 10. Same as Fig. 9, except for $e^+$ impact.

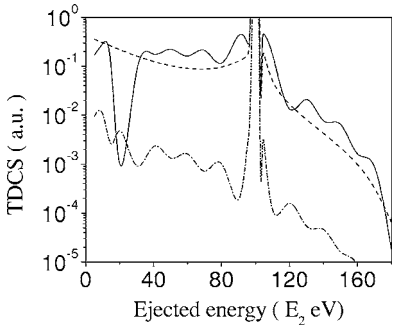


FIG. 11. $e^+$ impact laser-assisted ($l=0$) TDCS versus the ejected energy ($E_2$ in eV) distribution. $E_i=254.4$ eV, $\theta_1=3°$, and $\theta_2=0°$. Laser parameters are same as in Figs. 1–4. Solid curve: LM1 results, dash-dot curve: LM0 results, dashed curve: FF TDCS.

involving the electron positron correlation term (attractive) is responsible for such strong forward peak. In contrast, for $e$ impact (Fig. 9), the same Coulomb density of states factor that accounts for the Coulomb repulsion between the scattered and ionized electron, gives rise to an exponentially vanishing cross section (Fig. 9) when the two outgoing electron emerge with equal velocity.

Figure 11 illustrates the laser-assisted TDCS against the ejected electron energy ($E_2$) along with the corresponding FF results for single-photon absorption ($l=1$) at an incident energy $E_i=254.4$ eV when the $e^+$ and the ejected electron emerge almost in the same direction ($\theta_1=3°$, $\theta_2=0°$, $\phi_1=\phi_2=0°$). As is quite apparent from the figure, the TDCS exhibits a sharp ECC asymmetric cusp both with and without the laser field at half the residual energy ($E_1=E_2=E_r/2$). In fact, the qualitative nature of the FF ECC cusp is not changed drastically in presence of the field, except for some oscillations. However, quantitatively the overall TDCS magnitude is increased in the LM1 case and decreased (significantly) in the LM0 case with respect to the FF one.

Figures 12 and 13 illustrate the laser-assisted single-photon transfer ($l=1$) TDCS (LM1) for different frequencies at an incident energy $E_i=250$ eV for $e$ (Fig. 12) and $e^+$ (Fig. 13) impact. For this particular study, the laser frequencies are

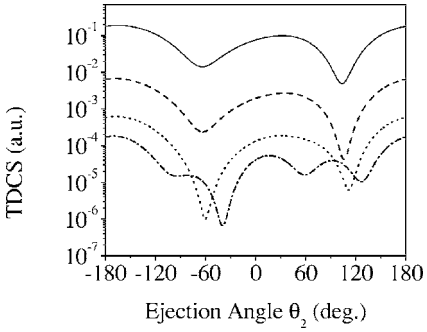


FIG. 12. $e$ impact laser assisted ($l=1$) TDCS versus the ejection angle $\theta_2$ for different laser frequencies with field strength $\varepsilon_0=5\times10^9$ V/m. $E_i=250$ eV, $E_2=5$ eV, $\theta_1=3°$. Dashed curve: LM1 TDCS for $\omega=3.406$ eV, dotted curve: LM1 TDCS for $\omega=6.42$ eV and dash-dot curve: LM1 TDCS for $\omega=10.2$ eV. Solid curve: FF results.

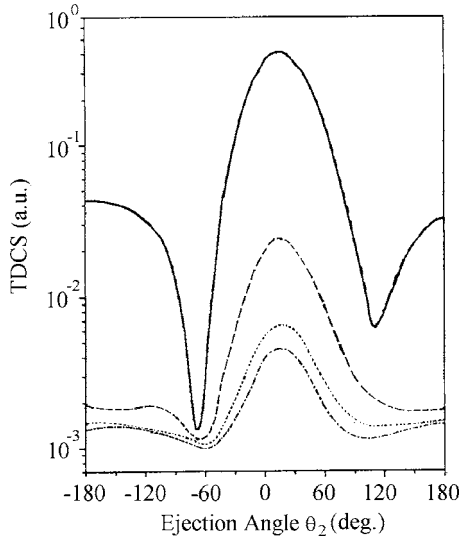


FIG. 13. Same as Fig. 12, except for $e^+$ impact.

chosen to be 3.406 eV (argon laser, near-UV region), 6.42 eV (ArF laser, far-ultraviolet region), 10.2 eV (Hg vapor laser, VUV region), while the laser field strength is kept unchanged ($5\times10^9$ V/m). As is evident from the figures, the magnitude of the laser-assisted TDCS decreases with increasing laser frequency ($\omega$) for both $e$ and $e^+$ impact indicating that there is a strong suppression in the ionization phenomena at high laser frequency, e.g., at $\omega=10.2$ eV, the TDCS peak intensities are reduced almost by three orders of magnitude with respect to the FF case.

Figures 14 and 15 demonstrate the variation of the TDCS with respect to the initial phase ($\delta=0°-180°$) of the laser field at $E_i=250$ eV for $e$ (Fig. 14) and $e^+$ (Fig. 15) impact, other parameters remaining same as in Figs. 1–4. All the TDCS results in Figs. 12 and 13 correspond to the first-order dressing of the ejected electron (LM1). As is evident from the Fig. 14 that for electron impact, the TDCS with $\delta=0°$, 90°, and 180° coincide with each other as is also followed

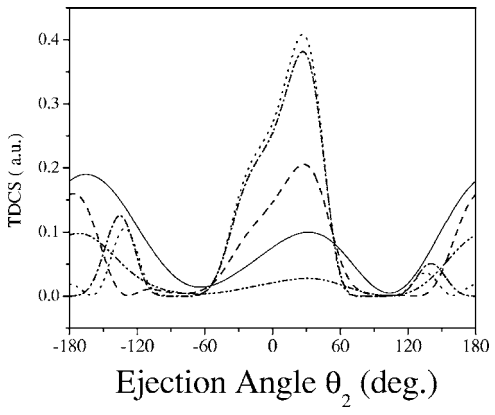


FIG. 14. Variation of the $e$ impact TDCS (versus $\theta_2$) for different values of the initial phase $\delta$ of the laser field (for $l=1$) and for LM1 case. $E_i=250$ eV, other parameters are same as in Figs. 1–4. The dashed curve: LM1 TDCS with $\delta=0°$, 90°, or 180°, dotted curve: TDCS with $\delta=45°$, dash-dot curve: TDCS with $\delta=60°$, dash-dot-dot curve: TDCS with $\delta=120°$, solid curve: FF results.

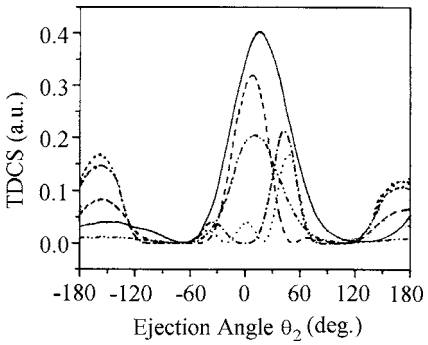


FIG. 15. Same as Fig. 14, except for $e^+$ impact.

from the theory. On the other hand, for the other values of $\delta$, e.g., $\delta=45°$ and 60°, the binary peaks lie much above the zero phase ($\delta=0$) peak as well as the FF binary peak with the exception at $\delta=120°$, where a reverse behavior is noted, e.g., the binary peak lies below the zero phase as well as the FF binary peaks. In the recoil region, on the other hand, the results for all other $\delta$'s are less than those for the FF case.

The situation is almost reverse in the case of $e^+$ impact (Fig. 15). For instance, the binary peaks of the TDCS with all phases lie below the FF one. Further, the results with $\delta=0°$, 90°, or 180° (being identical with each other) are much more high than those for other phases e.g., $\delta=45°$, 60°, and 120°. As for the recoil peaks for $e^+$ impact, the laser-assisted results with all values of $\delta$, except $\delta=120°$ are enhanced with respect to the FF case.

Finally, comparison between Figs. 14 and 15 reveal that the TDCS is much more sensitive with respect to $\delta$ in the binary region for $e$ impact and in the recoil region for $e^+$ impact.

## IV. CONCLUSIONS

The salient features of the present study are outlined below.

In the zeroth-order dressing of the ejected electron (LM0) the laser modification on the TDCS is much more effective in the recoil (binary) region for electron (positron) impact, while in the first-order dressing (LM1), both binary and recoil peaks are modified significantly.

A large discrepancy is noted in the zeroth- (LM0) and first-order (LM1) results. The overall effect of the laser field on the TDCS is to suppress the cross sections in the LM0 case both for $e$ and $e^+$ impact. The modification on the LM1 case is highly sensitive to the kinematics of the process.

The strong recoil (binary) peak for electron (positron) impact ionization of an ionic target is not retained in presence of the laser field. The FF $b/r$ ratio is modified significantly by the laser field.

For $e^+$ impact, the spread of the ECC cusp (in the velocity space around $v_p \approx v_e$) is increased in presence of the field (LM1).

With increasing laser frequency, the laser-assisted TDCS results get suppressed. More is the frequency, less is the cross section.

The TDCS is found to be quite sensitive with respect to the initial phase ($\delta$) of the laser field, particularly the binary (recoil) region for electron (positron) impact.

Improvement over the present calculation, using closure approximation in the dressed continuum wave function of the ejected electron could be ventured in a future work.

[1] A. Weingartshofer, J. K. Holmes, G. Caudle, E. M. Clarke, and H. Kruger, Phys. Rev. Lett. **39**, 269 (1977).
[2] A. Weingartshofer, E. M. Clarke, J. K. Holmes, and C. Jung, Phys. Rev. A **19**, 2371 (1979).
[3] N. J. Mason and W. R. Newell, J. Phys. B **20**, 1357 (1987).
[4] N. J. Mason and W. R. Newell, J. Phys. B **22**, 777 (1989).
[5] B. Wallbank, J. K. Holmes, and A. Weingartshofer, J. Phys. B **23**, 2997 (1990).
[6] S. Luan, R. Hippler, and H. O. Lutz, J. Phys. B **24**, 3241 (1991).
[7] B. Wallbank, J. K. Holmes, S. Maclsaac, and A. Weingartshofer, J. Phys. B **25**, 1265 (1992).
[8] B. Wallbank and J. K. Holmes, J. Phys. B **27**, 1221 (1994).
[9] B. Wallbank and J. K. Holmes, J. Phys. B **27**, 5405 (1994).
[10] C. Höhr, A. Dorn, B. Najjari, D. Fischer, C. D. Schröter, and J. Ullrich, Phys. Rev. Lett. **94**, 153201 (2005).
[11] P. Cavaliere, G. Ferrante, and C. Leone, J. Phys. B **13**, 4495 (1980).
[12] J. Banerji and M. H. Mittleman, J. Phys. B **14**, 3717 (1981).
[13] R. Zangara, P. Cavaliere, C. Leone, and G. Ferrante, J. Phys. B **15**, 3881 (1982).
[14] C. J. Joachain, P. Francken, A. Maquet, P. Martin, and V. Veniard, Phys. Rev. Lett. **61**, 165 (1988).
[15] P. Martin, V. Veniard, A. Maquet, P. Francken, and C. J. Joachain, Phys. Rev. A **39**, 6178 (1989).
[16] D. Khalil, A. Maquet, R. Taïeb, C. J. Joachain, and A. Makhoute, Phys. Rev. A **56**, 4918 (1997).
[17] S. M. Li, J. Chen, and Z. F. Zhou, J. Phys. B **35**, 557 (2002).
[18] G. Duchateau, E. Cormier, and R. Gayet, Phys. Rev. A **66**, 023412 (2002).
[19] J. Ullrich, R. Moshammer, A. Dorn, R. Dörner, L. P. H. Schmidt, and H. Schmidt-Böcking, Rep. Prog. Phys. **66**, 1463 (2003).
[20] M. Brauner, J. S. Briggs, and H. Klar, J. Phys. B **22**, 2265 (1989).
[21] M. Jain and N. Tzoar, Phys. Rev. A **18**, 538 (1978).
[22] A. Chattopadhyay and C. Sinha, J. Phys. B **37**, 3283 (2004).
[23] M. Bhattacharya, C. Sinha, and N. C. Sil, Phys. Rev. A **44**, 1884 (1991).
[24] G. Ferrante, C. Leone, and F. Trombetta, J. Phys. B **15**, L475 (1982).
[25] O. El Akramine, A. Makhoute, D. Khalil, A. Maquet, and R. Taïeb, J. Phys. B **32**, 2783 (1999).
[26] A. Makhoute, D. Khalil, A. Maquet, C. J. Joachain, and R. Taïeb, J. Phys. B **32**, 3255 (1999).
[27] L. Rosenberg, Adv. At. Mol. Phys. **18**, 1 (1982).

[28] F. H. M. Faisal, *Theory of Multiphoton Processes* (Plenum, New York, 1987).
[29] M. Dörr, C. J. Joachain, R. M. Potvliege, and S. Vucic, Phys. Rev. A **49**, 4852 (1994).
[30] F. W. Byron Jr., P. Francken, and C. J. Joachain, J. Phys. B **20**, 5487 (1987).
[31] W. G. Wan and J. Chen, J. Phys. B **33**, 3185 (2000).
[32] A. Cionga, F. Ehlotzky, and G. Zloh, Phys. Rev. A **64**, 043401 (2001).
[33] G. N. Watson, *A Treatise on the Theory of Bessel Functions*, 2nd ed. (Cambridge University Press, Cambridge, U.K., 1944).
[34] R. Biswas and C. Sinha, Phys. Rev. A **50**, 354 (1994).
[35] R. Biswas and C. Sinha, J. Phys. B **30**, 1589 (1997).
[36] B. Nath, S. Chattopadhyaya, and C. Sinha, Eur. Phys. J. D **11**, 31 (2000).